

A New Least Squares Stabilized Nitsche Method for Cut Isogeometric Analysis

Daniel Elfverson, Mats G. Larson and Karl Larsson

Abstract

We derive a new stabilized symmetric Nitsche method for enforcement of Dirichlet boundary conditions for elliptic problems of second order in cut isogeometric analysis (CutIGA). We consider C^1 splines and stabilize the standard Nitsche method by adding certain elementwise least squares terms in the vicinity of the Dirichlet boundary and an additional term on the boundary which involves the tangential gradient. We show coercivity with respect to the energy norm for functions in $H^2(\Omega)$ and optimal order a priori error estimates in the energy and L^2 norms. To obtain a well posed linear system of equations we combine our formulation with basis function removal which essentially eliminates basis functions with sufficiently small intersection with Ω . The upshot of the formulation is that only elementwise stabilization is added in contrast to standard procedures based on ghost penalty and related techniques and that the stabilization is consistent. In our numerical experiments we see that the method works remarkably well in even extreme cut situations using a Nitsche parameter of moderate size.

1 Introduction

Earlier Work. Cut finite element methods allow the geometric description of the computational domain to cut through the mesh in an arbitrary way. The resulting cut elements lead to difficulties on the Dirichlet boundary. Typically three approaches are used to handle this situation:

- Symmetric Nitsche in combination with stabilization using ghost penalties [4] and for the higher order case [16] or element merging [1] and [14] which ensures that the necessary inverse inequality holds to guarantee coercivity.
- Symmetric Nitsche in combination with a sufficiently large value of the Nitsche parameter to ensure coercivity, see for instance [8] and [7]. This approach can also be combined with some stabilization for instance of finite cell type [18] where a small amount of added stiffness is added to the full element.
- Nonsymmetric Nitsche, see [17], which avoids the use of the inverse inequality to establish coercivity. Note however that some additional stabilization is necessary to establish a priori error estimates, see [10] for details.

The first alternative rests on a complete theoretical basis; the second is common in practice but optimal order a priori bounds can not be established in general since the penalty parameter may become very large, see the discussion in [7]; and the third alternative was

considered in [10] where a least squares term was added in the vicinity of the Dirichlet part of the boundary to provide the additional stability necessary to establish a priori error bounds.

We refer to the overview article [5], and the recent conference proceedings [3] for an overview of current research on cut element methods.

New Contributions. In this paper we develop a new symmetric Nitsche formulation for cut C^1 elements that is coercive but does not rely on ghost penalties or choosing a very large penalty parameter in the Nitsche penalty term. The method is instead based on adding two properly scaled consistent least squares terms. First one term on elements in the vicinity of the boundary and second one term which provides control of the tangent gradient along the boundary. The latter term is related to enforcement of the Dirichlet boundary condition in $H^{1/2}(\partial\Omega)$, where Ω is the computational domain with boundary $\partial\Omega$. On standard elements which are not cut we may apply an inverse inequality and bound the least squares term involving the tangent gradient in terms of the standard Nitsche term but this is not possible on cut elements (unless some other stabilization is used). Therefore, on cut elements the stabilization term provides the additional control which reflects enforcement of the Dirichlet boundary condition in $H^{1/2}(\partial\Omega)$.

Together, these terms lead to a Nitsche formulation which is coercive with respect to the energy norm on $V = H^2(\Omega)$ in contrast to standard analysis of symmetric Nitsche which rely on inverse inequalities on the finite element space V_h . We utilize the added smoothness of the splines in our derivations and therefore only consider finite element spaces with at least C^1 regularity. The bulk part of the new least squares stabilization was used in [10] in combination with the non symmetric Nitsche formulation. Here we show that adding some additional stabilization also on the boundary leads to a natural extension of these results to the symmetric Nitsche formulation. Another interesting aspect of the new method is that we obtain explicit values of the stabilization parameters including the Nitsche parameter.

We focus in particular on the B-spline spaces which are commonly used in isogeometric analysis [6] but our approach is applicable to other types of C^1 finite element spaces, for instance tensor products of Hermite splines.

Our formulation is coercive on $H^2(\Omega)$ but the stiffness matrix is only guaranteed to be positive semidefinite since we allow elements with arbitrarily small intersection with the domain Ω . In order to ensure that the stiffness matrix is positive definite we employ the recently introduced Basis Function Removal technique, see [10], which builds on the obvious idea of simply excluding basis functions with very small intersection. This can be done in such a way that accuracy is not lost.

In our numerical investigations the method produces convergence results which are remarkably stable with respect to the cut situation. Also, the Nitsche penalty parameter in this case can be kept at a moderate size, say 100, which avoids problems due to locking when the boundary is curved within cut elements or inhomogeneous boundary data.

Outline. The paper is organized as follows. In Section 2 we a model problem and introduce the stabilized Nitsche formulation. In Section 3 we prove stability and error estimates in the energy and L^2 norms. In Section 4 we present illustrating numerical examples which confirms the theoretical results.

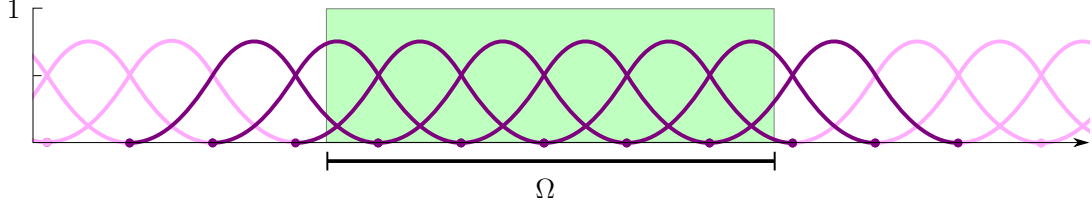


Figure 1: Quadratic B-spline basis functions in one dimension. The set B of basis functions with non-empty support in Ω are indicated in deep purple. Note that basis functions crossing the boundary of Ω are defined analogously to interior basis functions.

2 The Model Problem and Method

2.1 The Dirichlet Problem

Let Ω be a domain in \mathbb{R}^d with smooth boundary $\partial\Omega$ and consider the problem: find $u : \Omega \rightarrow \mathbb{R}$ such that

$$-\Delta u = f \quad \text{in } \Omega \quad (2.1)$$

$$u = g \quad \text{on } \partial\Omega \quad (2.2)$$

For sufficiently regular data there exists a unique solution to this problem and we will be interested in higher order methods and therefore we will always assume that the solution satisfies the regularity estimate

$$\|u\|_{H^s(\Omega)} \lesssim \|f\|_{H^{s-2}(\Omega)} + \|g\|_{H^{s-1/2}(\partial\Omega)} \quad (2.3)$$

for some $s \geq 2$. Here and below $a \lesssim b$ means that there is a positive constant C such that $a \leq Cb$.

2.2 The B-Spline Spaces

Definitions.

- Let $\tilde{\mathcal{T}}_h$, $h \in (0, h_0]$, for some constant $h_0 > 0$, be a family of uniform tensor product meshes in \mathbb{R}^d with mesh parameter h .
- Let $\tilde{V}_h = C^{p-1}Q^p(\mathbb{R}^d)$ be the space of C^{p-1} tensor product B-splines of order p defined on $\tilde{\mathcal{T}}_h$. Let $\tilde{B} = \{\varphi_i\}_{i \in \tilde{I}}$ be the standard basis in \tilde{V}_h , where \tilde{I} is an index set.
- Let $B = \{\varphi \in \tilde{B} : \text{supp}(\varphi) \cap \Omega \neq \emptyset\}$ be the set of basis functions with support that intersects Ω . Let I be an index set for B . Let $V_h = \text{span}\{B\}$ and let $\mathcal{T}_h = \{T \in \tilde{\mathcal{T}}_h : T \subset \cup_{\varphi \in B} \text{supp}(\varphi)\}$.
- We will only consider $p \geq 2$ corresponding to at least C^1 splines. We then have $V_h \subset V = H^2(\Omega)$. The case $p = 2$ in 1D is illustrated in Figure 1.

Remark 2.1. To construct the basis functions in \tilde{V}_h we start with the one dimensional line \mathbb{R} and define a uniform partition, with nodes $x_i = ih$, $i \in \mathbb{Z}$, where h is the mesh parameter, and elements $I_i = [x_{i-1}, x_i)$. We define

$$\varphi_{i,0}(x) = \begin{cases} 1 & x \in I_i \\ 0 & x \in \mathbb{R} \setminus I_i \end{cases} \quad (2.4)$$

The basis functions $\varphi_{i,p}$ are then defined by the Cox-de Boor recursion formula

$$\varphi_{i,p} = \frac{x - x_i}{x_{i+p} - x_i} \varphi_{i,p-1}(x) + \frac{x_{i+p+1} - x}{x_{i+p+1} - x_{i+1}} \varphi_{i+1,p-1}(x) \quad (2.5)$$

we note that these basis functions are C^{p-1} and supported on $[x_i, x_{i+p+1}]$ which corresponds to $p+1$ elements. We then define tensor product basis functions in \mathbb{R}^d of the form

$$\varphi_{i_1, \dots, i_d}(x) = \prod_{k=1}^d \varphi_{i_k}(x_k) \quad (2.6)$$

2.3 The Finite Element Method

Method. Find $u_h \in V_h$ such that

$$A_h(u_h, v) = L_h(v) \quad v \in V_h \quad (2.7)$$

Forms. Let $\delta \sim h$ be a parameter and define the forms

$$A_h(v, w) = a_h(v, w) - (n \cdot \nabla v, w)_{\partial\Omega} - (v, n \cdot \nabla w)_{\partial\Omega} + \beta b_h(v, w) \quad (2.8)$$

$$a_h(v, w) = (\nabla v, \nabla w)_{\Omega} + \tau \delta^2 (\Delta v, \Delta w)_{\mathcal{T}_{h,\delta} \cap \Omega} \quad (2.9)$$

$$b_h(v, w) = (1 + \tau^{-1}) \delta^{-1} (v, w)_{\partial\Omega} + \delta (\nabla_T v, \nabla_T w)_{\partial\Omega} \quad (2.10)$$

$$L_h(v) = (f, v)_{\Omega} - \tau \delta^2 (f, \Delta v)_{\mathcal{T}_{h,\delta} \cap \Omega} - (g, n \cdot \nabla v)_{\partial\Omega} + \beta b_h(g, v) \quad (2.11)$$

Here we used the notation:

- β is the penalty parameter which can take a moderate value for instance $5 \leq \beta$ and τ is a positive parameter which enables us the trade weight between the least squares bulk term and the standard Nitsche term. We note in practice that a small τ leads to a more accurate method. We refer to the numerical section for more details on the choice of parameters.
- ∇_T is the tangential gradient at $\partial\Omega$ defined by $\nabla_T = P\nabla$, where $P = I - n \otimes n$ is the projection of vectors in \mathbb{R}^d onto the tangent plane of the boundary $\partial\Omega$.
- In (2.9) we used the form

$$(v, w)_{\mathcal{T}_{h,\delta} \cap \Omega} = \sum_{T \in \mathcal{T}_{h,\delta}} (v, w)_{T \cap \Omega} \quad (2.12)$$

where $\mathcal{T}_{h,\delta} \subset \mathcal{T}_h$ is defined by

$$\mathcal{T}_{h,\delta} = \mathcal{T}_h(U_{\delta}(\partial\Omega)) = \{T \in \mathcal{T}_h : T \cap U_{\delta}(\partial\Omega) \neq \emptyset\} \quad (2.13)$$

and

$$U_{\delta}(\partial\Omega) = \left(\bigcup_{x \in \partial\Omega} B_{\delta}(x) \right) \cap \Omega \quad (2.14)$$

with $\delta \sim h$ and $B_{\delta}(x)$ the open ball with center x and radius δ . See Figure 2 for an illustration.

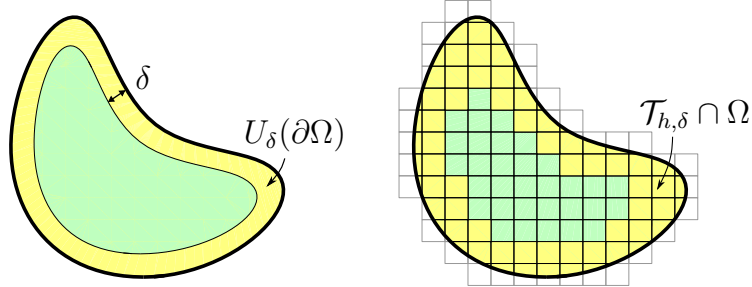


Figure 2: Illustrations of subdomains $U_\delta(\partial\Omega)$ and $\mathcal{T}_{h,\delta} \cap \Omega$ where $\mathcal{T}_{h,\delta}$ is extracted according to Remark 2.2.

Galerkin Orthogonality. It holds

$$A_h(u - u_h, v) = 0 \quad \forall v \in V_h \quad (2.15)$$

This identity follows directly from the consistency of the standard Nitsche method and the fact that we have only added consistent least squares terms.

Remark 2.2. In practice, if $\delta = h$ is used $\mathcal{T}_{h,\delta}$ may be taken as the set of all elements that intersect the Dirichlet boundary $\partial\Omega$ and their neighbors, i.e. $\mathcal{T}_{h,\delta} = \mathcal{N}_h(\mathcal{T}_h(\partial\Omega))$, see Figure 2.

Remark 2.3. We note that in addition to the usual Nitsche formulation we have an interior least squares term and also a term providing control of the tangent derivative along the boundary. Both of these terms can be computed elementwise using the standard assembly of the stiffness matrix. Note also that the stabilization terms do not cause fill in which is the case with standard ghost penalty approaches [4, 15, 16].

3 Error Estimates

3.1 Properties of A_h

Norms. Define the norms

$$\|v\|_h^2 = \|v\|_{a_h}^2 + \|v\|_{b_h}^2 \quad (3.1)$$

$$\|v\|_{a_h}^2 = a_h(v, v) = \|\nabla v\|_\Omega^2 + \tau\delta^2 \|\Delta v\|_{\mathcal{T}_{h,\delta} \cap \Omega}^2 \quad (3.2)$$

$$\|v\|_{b_h}^2 = b_h(v, v) = (1 + \tau^{-1})\delta^{-1} \|v\|_{\partial\Omega}^2 + \delta \|\nabla_T v\|_{\partial\Omega}^2 \quad (3.3)$$

Technical Lemmas. Let ρ , with $\rho > 0$ in Ω , be the signed distance function associated with $\partial\Omega$ and recall that the closest point mapping $p : U_\delta \rightarrow \partial\Omega$ is well defined for $0 < \delta \leq \delta_0$ where

$$\delta_0 \|\kappa\|_{L^\infty(\partial\Omega)} \leq C_1 < 1 \quad (3.4)$$

Here $\kappa = \nabla^2 \rho$ is the curvature tensor of $\partial\Omega$ and $\|\kappa\|_{L^\infty(\partial\Omega)} = \sup_{x \in \partial\Omega} \|\kappa\|_{\mathbb{R}^d}$ where $\|\cdot\|_{\mathbb{R}^d}$ on a $d \times d$ matrix is the operator norm. See [12] for further details. Through the closest point mapping we extend functions v defined on $\partial\Omega$ onto U_δ and we use the notation

$$v^e = v \circ p \quad (3.5)$$

Furthermore, we will let C denote constants independent of the mesh, the domain, and the intersection between the domain and the mesh, which are not the same at all occurrences. An index is used to indicate the constant in a specific inequality.

We consider mesh parameters $h \in (0, h_0]$, and let δ be a parameter such that

$$0 < h \leq \delta \leq h_0 \leq \delta_0 \quad (3.6)$$

which essentially means that the mesh resolves the boundary.

Lemma 3.1. *Let δ satisfy (3.4), then*

$$\|v^e\|_{U_\delta}^2 \lesssim \delta \|v\|_{\partial\Omega}^2 \quad (3.7)$$

$$\|\nabla v^e\|_{U_\delta}^2 \lesssim \delta \|\nabla_T v\|_{\partial\Omega}^2 \quad (3.8)$$

where the hidden constant takes the form $1 + C\delta\|\kappa\|_{L^\infty(\partial\Omega)}$.

Proof. For $t \in (0, \delta_0)$ we define $\partial\Omega_t = \{x \in \Omega : \rho(x) = t\}$. Let dx_t be the surface measure on $\partial\Omega_t$. Then we have $dx_t = \mu_t dx$, where dx is the surface measure on $\partial\Omega$, and the following estimate

$$\|\mu_t\|_{L^\infty(\partial\Omega)} \leq 1 + Ct\|\kappa\|_{L^\infty(\partial\Omega)} \quad (3.9)$$

(3.7) Using (3.9) we obtain

$$\|w^e\|_{U_\delta}^2 = \int_0^\delta \|w^e\|_{\partial\Omega_t}^2 dt \quad (3.10)$$

$$= \int_0^\delta \int_{\partial\Omega_t} |w^e|^2 dx_t dt \quad (3.11)$$

$$= \int_0^\delta \int_{\partial\Omega} |w|^2 \mu_t dx dt \quad (3.12)$$

$$\leq \int_0^\delta (1 + Ct\|\kappa\|_{L^\infty(\partial\Omega)}) dt \int_{\partial\Omega} |w|^2 dx \quad (3.13)$$

$$= \delta \left(1 + C\frac{\delta}{2}\|\kappa\|_{L^\infty(\partial\Omega)} \right) \|w\|_{\partial\Omega}^2 \quad (3.14)$$

(3.8). Using the chain rule we have

$$(\nabla v^e)|_x = (Dp|_x)^T (\nabla v)|_{p(x)} = (I + \rho(x)\kappa(x))^T (P\nabla v)|_{p(x)} \quad (3.15)$$

where $Dp(x) = I - n(p(x)) \otimes n(p(x)) - \rho(x)\kappa(x)$ is the Jacobian of the closest point mapping. Thus we obtain the estimate

$$\|\nabla v^e(x)\|_{\mathbb{R}^d} \leq \|I + \rho(x)\kappa(x)\|_{\mathbb{R}^d} \|(\nabla_T v)^e\|_{\mathbb{R}^d} \leq (1 + \rho(x)\|\kappa(x)\|_{\mathbb{R}^d}) \|(\nabla_T v)^e\|_{\mathbb{R}^d} \quad (3.16)$$

where $\|\kappa(x)\|_{\mathbb{R}^d} \leq (1 - C_1)^{-1} \|\kappa(p(x))\|_{\mathbb{R}^d} \leq C \|\kappa(p(x))\|_{\mathbb{R}^d}$, and C_1 is the constant in (3.4), which we may take to $1/2$ for instance. We thus have

$$\|\nabla v^e(x)\|_{\mathbb{R}^d} \leq \left(1 + C\rho(x)\|\kappa\|_{L^\infty(\partial\Omega)} \right) \|(\nabla_T v)^e\|_{\mathbb{R}^d} \quad x \in U_\delta \quad (3.17)$$

We now estimate the integral in as follows

$$\|\nabla w^e\|_{U_\delta}^2 = \int_0^\delta \|\nabla w^e\|_{\partial\Omega_t}^2 dt \quad (3.18)$$

$$= \int_0^\delta \int_{\partial\Omega_t} \|\nabla w^e\|_{\mathbb{R}^d}^2 dx_t dt \quad (3.19)$$

$$= \int_0^\delta \int_{\partial\Omega_t} \|(I + t\kappa)(\nabla_T w)^e\|_{\mathbb{R}^d}^2 dx_t dt \quad (3.20)$$

$$\leq \int_0^\delta (1 + Ct\|\kappa\|_{L^\infty(\partial\Omega)})(1 + Ct\|\kappa\|_{L^\infty(\partial\Omega)})^2 dt \int_{\partial\Omega} \|\nabla_T v\|_{\mathbb{R}^d}^2 dx \quad (3.21)$$

$$\lesssim \delta \left(1 + C\delta\|\kappa\|_{L^\infty(\partial\Omega)}\right) \|\nabla_T w\|_{\partial\Omega}^2 \quad (3.22)$$

Here we used the estimate

$$\int_0^\delta (1 + Ct\|\kappa\|_{L^\infty(\partial\Omega)})(1 + Ct\|\kappa\|_{L^\infty(\partial\Omega)})^2 dt \quad (3.23)$$

$$= \int_0^\delta 1 + 3Ct\|\kappa\|_{L^\infty(\partial\Omega)} + 3(Ct)^2\|\kappa\|_{L^\infty(\partial\Omega)}^2 + (Ct)^3\|\kappa\|_{L^\infty(\partial\Omega)}^3 dt \quad (3.24)$$

$$= \delta \left(1 + \frac{3}{2}C\delta\|\kappa\|_{L^\infty(\partial\Omega)} + (C\delta)^2\|\kappa\|_{L^\infty(\partial\Omega)}^2 + \frac{1}{4}(C\delta)^3\|\kappa\|_{L^\infty(\partial\Omega)}^3\right) \quad (3.25)$$

$$\lesssim \delta \left(1 + C\delta\|\kappa\|_{L^\infty(\partial\Omega)}\right) \quad (3.26)$$

where we at last used (3.4). ■

Lemma 3.2. *The following estimate holds*

$$(n \cdot \nabla v, w)_{\partial\Omega} \lesssim \|v\|_{a_h} \|w\|_{b_h} \quad v, w \in V \quad (3.27)$$

Proof. Given $\delta > 0$ let $\chi : \Omega \rightarrow [0, 1]$ be defined by

$$\chi(x) = \begin{cases} 1 - \rho(x)/\delta & x \in U_\delta \\ 0 & x \in \Omega \setminus U_\delta \end{cases} \quad (3.28)$$

Then we have

$$\|\chi\|_{L^\infty(\Omega)} = 1, \quad \|\nabla\chi\|_{L^\infty(\Omega)} = 1/\delta \quad (3.29)$$

Using Green's formula we have the identity

$$(\nabla v, \chi \nabla w^e)_{U_\delta} = (n \cdot \nabla v, \chi w^e)_{\partial\Omega} - (\Delta v, \chi w^e)_{U_\delta} - (\nabla v, (\nabla\chi)w^e)_{U_\delta} \quad (3.30)$$

Rearranging the terms and estimating

$$(n \cdot \nabla v, \chi w^e)_{\partial\Omega} = (\nabla v, \chi \nabla w^e)_{U_\delta} + (\Delta v, \chi w^e)_{U_\delta} + (\nabla v, (\nabla\chi)w^e)_{U_\delta} \quad (3.31)$$

$$\leq \|\nabla v\|_{U_\delta} \|\nabla w^e\|_{U_\delta} + \tau^{1/2}\delta \|\Delta v\|_{U_\delta} \tau^{-1/2}\delta^{-1} \|w^e\|_{U_\delta} + \|\nabla v\|_{U_\delta} \delta^{-1} \|w^e\|_{U_\delta} \quad (3.32)$$

$$\lesssim \left(\|\nabla v\|_{U_\delta}^2 + \tau\delta^2 \|\Delta v\|_{U_\delta}^2\right)^{1/2} \left((1 + \tau^{-1})\delta^{-2} \|w^e\|_{U_\delta}^2 + \|\nabla w^e\|_{U_\delta}^2\right)^{1/2} \quad (3.33)$$

$$\lesssim \left(\|\nabla v\|_{U_\delta}^2 + \tau\delta^2 \|\Delta v\|_{U_\delta}^2\right)^{1/2} \left((1 + \tau^{-1})\delta^{-1} \|w\|_{\partial\Omega}^2 + \delta \|\nabla_T w\|_{\partial\Omega}^2\right)^{1/2} \quad (3.34)$$

Thus we finally arrive at

$$(n \cdot \nabla v, w)_{\partial\Omega} \lesssim \left(\|\nabla v\|_{U_\delta}^2 + \delta^2 \|\Delta v\|_{U_\delta}^2\right)^{1/2} (\delta^{-1} \|w\|_{\partial\Omega}^2 + \delta \|\nabla_T w\|_{\partial\Omega}^2)^{1/2} \quad (3.35)$$

and, taking $\delta \sim h$ gives the desired estimate. ■

Lemma 3.3. (Coercivity) For $\beta > 0$ sufficiently large the form A_h is coercive

$$\|v\|_h^2 \lesssim A_h(v, v) \quad v \in V \quad (3.36)$$

where $V = H^2(\Omega)$.

Remark 3.1. Note that the coercivity with respect to the energy norm holds on the full space $V = H^2(\Omega)$ and not only on the discrete space V_h . The reason is of course that we do not invoke any inverse inequality in the proof of the continuity bound (3.27).

Proof. We have

$$A_h(v, v) = \|v\|_{a_h}^2 - 2(n \cdot \nabla v, v)_{\partial\Omega} + \beta h^{-1} \|v\|_{b_h}^2 \quad (3.37)$$

$$\geq \|v\|_{a_h}^2 - 2C \|v\|_{a_h} \|v\|_{b_h} + \beta h^{-1} \|v\|_{b_h}^2 \quad (3.38)$$

$$\geq (1 - \gamma C) \|v\|_{a_h}^2 + (\beta - \gamma^{-1} C) \|v\|_{b_h}^2 \quad (3.39)$$

where C is the hidden constant in the continuity inequality (3.27). \blacksquare

Remark 3.2. The constant C is of very moderate size in fact it is close to one and approaches one as the meshsize tends to zero. Therefore the constant β may be chosen to have a moderate value, for instance we may take $5 \leq \beta$.

Lemma 3.4. (Continuity). The form A_h is continuous

$$A_h(v, w) \lesssim \|v\|_h \|w\|_h \quad v, w \in V \quad (3.40)$$

Proof. We have

$$A_h(v, w) = a_h(v, w) - (n \cdot \nabla v, w)_{\partial\Omega} - (v, n \cdot \nabla w)_{\partial\Omega} + b_h(v, w) \quad (3.41)$$

$$\lesssim \|v\|_{a_h} \|w\|_{a_h} + \|v\|_{a_h} \|w\|_{b_h} + \|v\|_{b_h} \|w\|_{a_h} + \|v\|_{b_h} \|w\|_{b_h} \quad (3.42)$$

$$\lesssim (\|v\|_{a_h}^2 + \|v\|_{b_h}^2)^{1/2} (\|w\|_{a_h}^2 + \|w\|_{b_h}^2)^{1/2} \quad (3.43)$$

$$\lesssim \|v\|_h \|w\|_h \quad (3.44)$$

where we used the trace inequality (3.27) followed by the Cauchy-Schwarz inequality. \blacksquare

3.2 Interpolation Error Estimates

There is an extension operator $E : W_q^k(\Omega) \rightarrow W_q^k(\mathbb{R}^d)$, $k \geq 0$ and $q \geq 1$, such that

$$\|Ev\|_{W_q^k(\mathbb{R}^d)} \lesssim \|v\|_{W_q^k(\Omega)} \quad (3.45)$$

see [11]. Define the interpolant by

$$\pi_h : H^s(\Omega) \ni u \mapsto \pi_{Cl,h}(Eu) \in V_h \quad (3.46)$$

where $\pi_{Cl,h}$ is a Clement type interpolation operator onto the spline space V_h . We have the standard a priori error estimate

$$\|v - \pi_h v\|_{H^m(T)} \lesssim h^{s-m} \|v\|_{H^s(\mathcal{N}_h(T))} \quad (3.47)$$

where $\mathcal{N}_h(T) = \cup_{\varphi \in B(T)} \text{supp}(\varphi)$ and $B(T) = \{\varphi \in B : T \subset \text{supp}(\varphi)\}$. See [2] for interpolation results for spline spaces.

Lemma 3.5. *We have the interpolation estimate*

$$\|v - \pi_h v\|_h \lesssim h^p \|v\|_{H^{p+1}(\Omega)} \quad (3.48)$$

for $0 \leq m \leq s \leq p + 1$.

Proof. We directly have the estimates

$$\|\nabla(v - \pi_h v)\|_{\Omega}^2 \lesssim h^{2p} \|v\|_{H^{p+1}(\Omega)}^2 \quad (3.49)$$

$$h^2 \|\Delta(v - \pi_h v)\|_{\Omega}^2 \lesssim h^{2p} \|v\|_{H^{p+1}(\Omega)}^2 \quad (3.50)$$

For the boundary terms we employ the trace inequality

$$\|v\|_{\partial\Omega}^2 \lesssim h^{-1} \|v\|_{\mathcal{T}_h(\partial\Omega)}^2 + h \|\nabla v\|_{\mathcal{T}_h(\partial\Omega)}^2 \quad (3.51)$$

see [13], which together with the interpolation bound (3.47) and the stability of the extension operator (3.45) give

$$h^{-1} \|v - \pi_h v\|_{\partial\Omega}^2 \lesssim h^2 \|v - \pi_h v\|_{\mathcal{T}_h(\partial\Omega)}^2 + \|\nabla(v - \pi_h v)\|_{\mathcal{T}_h(\partial\Omega)}^2 \quad (3.52)$$

$$\lesssim h^{2p} \|v\|_{H^{p+1}(\mathcal{N}_h(\mathcal{T}_h(\partial\Omega)))}^2 \quad (3.53)$$

$$\lesssim h^{2p} \|v\|_{H^{p+1}(\Omega)}^2 \quad (3.54)$$

$$h \|\nabla_T(v - \pi_h v)\|_{\partial\Omega}^2 \lesssim \|\nabla(v - \pi_h v)\|_{\mathcal{T}_h(\partial\Omega)}^2 + h^2 \|\nabla^2(v - \pi_h v)\|_{\mathcal{T}_h(\partial\Omega)}^2 \quad (3.55)$$

$$\lesssim h^{2p} \|v\|_{H^{p+1}(\mathcal{N}_h(\mathcal{T}_h(\partial\Omega)))}^2 \quad (3.56)$$

$$\lesssim h^{2p} \|v\|_{H^{p+1}(\Omega)}^2 \quad (3.57)$$

Summing these four bounds we directly obtain (3.48). ■

3.3 Error Estimates

Theorem 3.1. *The following error estimates holds*

$$\|u - u_h\|_h \lesssim h^p \|u\|_{H^{p+1}(\Omega)} \quad (3.58)$$

$$\|u - u_h\|_{\Omega} \lesssim h^{p+1} \|u\|_{H^{p+1}(\Omega)} \quad (3.59)$$

Proof. Estimate (3.58) follows directly from the coercivity, the Galerkin orthogonality (2.15), the continuity and finally the interpolation error estimate. Estimate (3.59) follows from (3.58) using a standard duality argument. ■

4 Basis Function Removal

The stiffness matrix \widehat{A} is defined by

$$(\widehat{A}\widehat{v}, \widehat{w})_{\mathbb{R}^N} = A_h(v, w) \quad \forall v, w \in V_h \quad (4.1)$$

where $\widehat{v} \in \mathbb{R}^N$ is the coefficient vector in the expansion

$$v(x) = \sum_{i \in I} \widehat{v}_i \varphi_i(x) \quad (4.2)$$

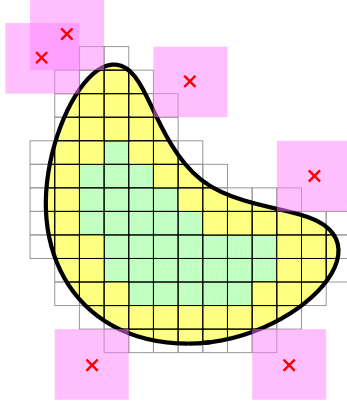


Figure 3: Illustration of quadratic B-spline basis functions selected for basis removal. For each selected basis function the location of its peak is indicated by a red cross and its support is indicated by a pink square.

of v in terms of the basis functions. We note that \hat{A} is symmetric and positive semidefinite since

$$(\hat{A}\hat{v}, \hat{v})_{\mathbb{R}^N} = A_h(v, v) \gtrsim \|v\|_h^2 \geq 0 \quad (4.3)$$

Note however that $\|v\|_h$ is only a semi norm on V_h since the functions in V_h are defined on $\Omega_h = \cup_{i \in I} \text{supp}(\varphi_i)$ and $\Omega \subset \Omega_h$ and there may be basis functions $\varphi \in B$ such that the intersection $\text{supp}(\varphi) \cap \Omega$ is arbitrarily small.

To obtain a positive definite stiffness matrix we apply basis function removal. This approach was analyzed in [10] and builds on the the idea of systematically removing basis functions that have sufficiently small intersection with the domain. This is done in such a way that optimal order accuracy in a specified norm is retained. For instance, using the energy norm we may remove basis functions according to the following procedure. Assuming the basis functions in $B = \{\varphi_i\}_{i=1}^N$ are sorted such that the size of their energy norms $\|\varphi_i\|_h$ are ascending we may remove the N_r first basis functions as long as

$$\sum_{i=1}^{N_r} \|\varphi_i\|_h^2 \leq \text{tol}^2 \quad (4.4)$$

with $\text{tol} = ch^p$. See Figure 3 for an example selection of basis functions. This natural procedure leads to optimal order convergence and a stiffness matrix which is uniformly symmetric positive definite independent of the position of the domain in the background mesh. We refer to [10] for further details. The resulting linear system of equations may then be solved using a direct solver or we may apply an iterative solver combined with a preconditioner. We refer to [8] and [9] for preconditioning of cut element methods.

5 Numerical Results

Implementation. The new least squares stabilized Nitsche method in 2D is implemented in MATLAB and the linear system of equations is solved using a direct solver (MATLAB's \backslash operator). We use tensor product quadratic B-spline basis functions, i.e. C^1 -splines, in all experiments. The domain Ω is described as a high resolution polygon. The additional terms, with regards to the standard symmetric Nitsche method which we formulate below, are added elementwise.

Parameter Values. In our experiments we let $\delta = h$ and extract the subdomain $\mathcal{T}_{h,\delta} \cap \Omega$ according to Remark 2.2. We use $\beta = 10$ while the value of $\tau > 0$ is varied. When basis removal is active we use a tolerance constant $c = 0.01$ as described in Section 4.

The Standard Symmetric Nitsche Method. For comparison we also include results for the standard symmetric Nitsche method defined via the forms

$$A_{h,\text{std}}(v, w) = (\nabla v, \nabla w)_\Omega - (n \cdot \nabla v, w)_{\partial\Omega} - (v, n \cdot \nabla w)_{\partial\Omega} + h^{-1}(\beta(1 + \tau^{-1})v, w)_{\partial\Omega} \quad (5.1)$$

$$L_{h,\text{std}}(v) = (f, v)_\Omega - (g, n \cdot \nabla v)_{\partial\Omega} + h^{-1}(\beta(1 + \tau^{-1})g, v)_{\partial\Omega} \quad (5.2)$$

To make for an easier comparison the Nitsche penalty parameter is written $\beta(1 + \tau^{-1})$ just as in our formulation of the least squares stabilized method (2.7).

Remark 5.1. *In the results below we in no way ensure coercivity of the standard symmetric Nitsche method. That could be performed using the techniques outlined in the introduction, for example by suitably increasing the penalty parameter. Thus, in examples below where the standard Nitsche method appears to perform poorly one could argue that this is a consequence of poor parameter choices for this method. However, we still found it interesting to include this comparison.*

5.1 Model Problems

We manufacture both our model problems based on the ansatz

$$u(x, y) = \frac{1}{10}(\sin(2x) + x \cos(3y)) \quad (5.3)$$

from which we, given a domain Ω , derive the input data f in Ω and $g, \nabla_T g$ on $\partial\Omega$.

Unit Square. The first geometry we consider is the unit square $\Omega = [0, 1]^2$ on which we examine both fitted meshes and cut meshes generated in a controlled fashion. The cut situations are created by letting the topmost and rightmost elements extend outside the domain a distance $h\delta_{\text{cut}}$. This is further described and illustrated in Figure 4. An example numerical solution to this model problem is shown in Figure 5. Note that we do not activate basis removal in the examples based on this model problem.

Unit Circle. As a second geometry we consider the unit circle $\Omega = \{x \in \mathbb{R}^2 : \|x\|_{\mathbb{R}^2} \leq 1\}$. This geometry will always produce cut situations on structured meshes. We produce a variety of cut situations by taking a background grid of size h and shifting it $(th, th/3)$ where t is a parameter. By letting the parameter t take 100 values ranging from 0 to 1, we yield 100 different cut situations for each mesh size h . Some example meshes generated using this procedure are presented in Figure 6 and an example numerical solution to this model problem is shown in Figure 7.

5.2 Experiments

Convergence Studies. We begin by studying convergence for the unit square problem on fitted meshes in Figure 8. Both the least squares stabilized Nitsche method and the

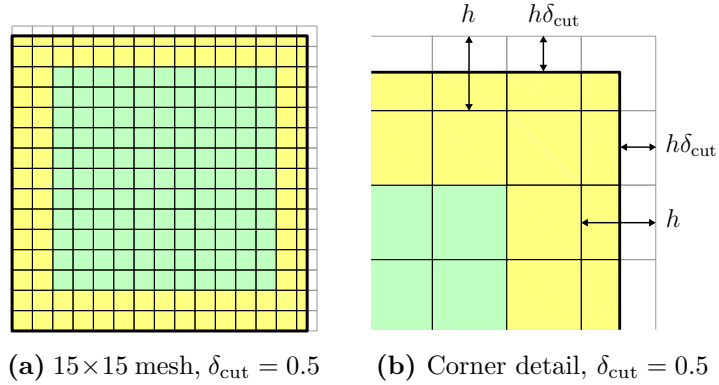


Figure 4: Example mesh for the unit square model problem. Here the geometry cuts through the mesh in a controlled fashion where the topmost and rightmost elements (aside from the corner) have a proportion δ_{cut} of their areas outside the domain. The case $\delta_{\text{cut}} = 0$ thus corresponds to a perfectly fitted mesh. The yellow part of the domain is $\mathcal{T}_{h,\delta} \cap \Omega$.

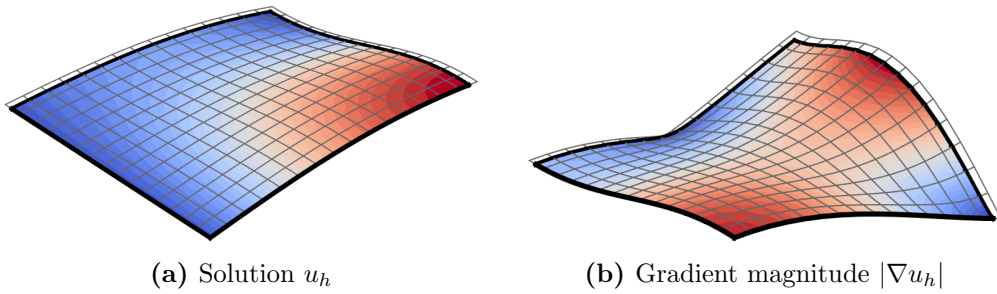


Figure 5: Example numerical solution to the unit square model problem using the least squares stabilized Nitsche method on the mesh in Figure 4.

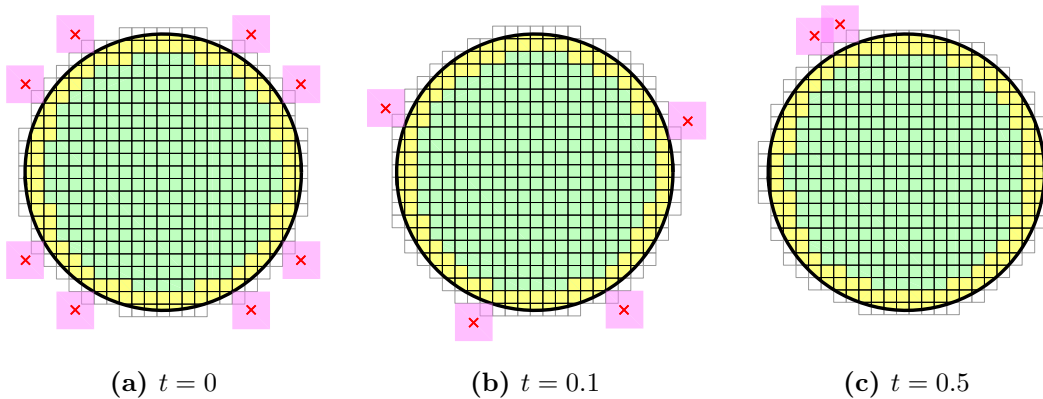


Figure 6: Example meshes ($h = 0.13$) for the unit circle. The background grid is shifted $(th, th/3)$ creating a variety of cut situations for each mesh size depending on the parameter t . The pink squares with a cross indicate the support of basis functions selected for basis removal using parameter values $c = 0.01$ and $\tau = 0.1$. The yellow part of the domain is $\mathcal{T}_{h,\delta} \cap \Omega$.

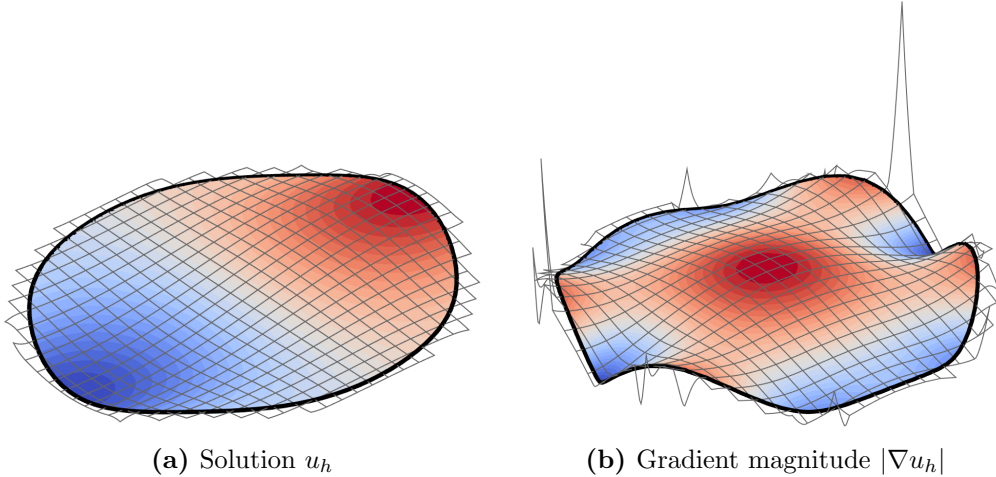


Figure 7: Example numerical solution to the unit circle model problem using the least squares stabilized Nitsche method on the mesh in Figure 6b.

standard Nitsche method perform well in for the tested parameter values albeit we initially see a slightly higher $L^2(\Omega)$ error for the least squares stabilized Nitsche method for $\tau = 1$. We attribute this to the $\mathcal{T}_{h,\delta} \cap \Omega$ least squares term which in addition to the imposed h^2 scaling also scales as the subdomain $\mathcal{T}_{h,\delta} \cap \Omega$ becomes smaller with h , explaining why we only note this on the coarsest meshes.

To study convergence on cut meshes we use the sequence of meshes specified for the unit circle problem. This gives access to a variety of cut situations and to illustrate the stability of the least squares stabilized Nitsche method we for each mesh size pick the largest errors among all available cut meshes, essentially producing a worst case scenario. These convergence results are presented in Figure 9 where the least squares stabilized Nitsche method show remarkable stability. For $\tau = 1$ we in the $L^2(\Omega)$ error initially note faster than expected convergence which we again attribute to the $\mathcal{T}_{h,\delta} \cap \Omega$ least squares term. For $\tau \geq 0.01$ the least squares stabilized Nitsche method and the standard Nitsche method produce visually indistinguishable convergence results. We note however that the size of the errors increase somewhat when further lowering τ and we investigate the performance of the methods for small values of τ in Figure 10. A smaller value for τ equates to a larger effective Nitsche penalty $\beta(1 + \tau^{-1})$ so we attribute this increasing error to locking due to inhomogeneous Dirichlet conditions and the fact that the boundary in the circle model problem is curved within each cut element. This latter property means that even homogeneous Dirichlet conditions cannot be exactly satisfied in our approximation space.

Condition Number Study. To illustrate the effect of basis function removal on the stiffness matrix condition number we use the unit circle model problem on a background grid of size $h = 0.13$ and shift this background grid in 100 steps as described above to create a variety of cut situations. The results from this study are presented in Figure 11. We note that the effect of basis function removal on the least squares stabilized Nitsche method seems stable for the tested values of τ while we note some minor instabilities when applying basis function removal on the standard Nitsche method for $\tau \in \{1, 0.1\}$.

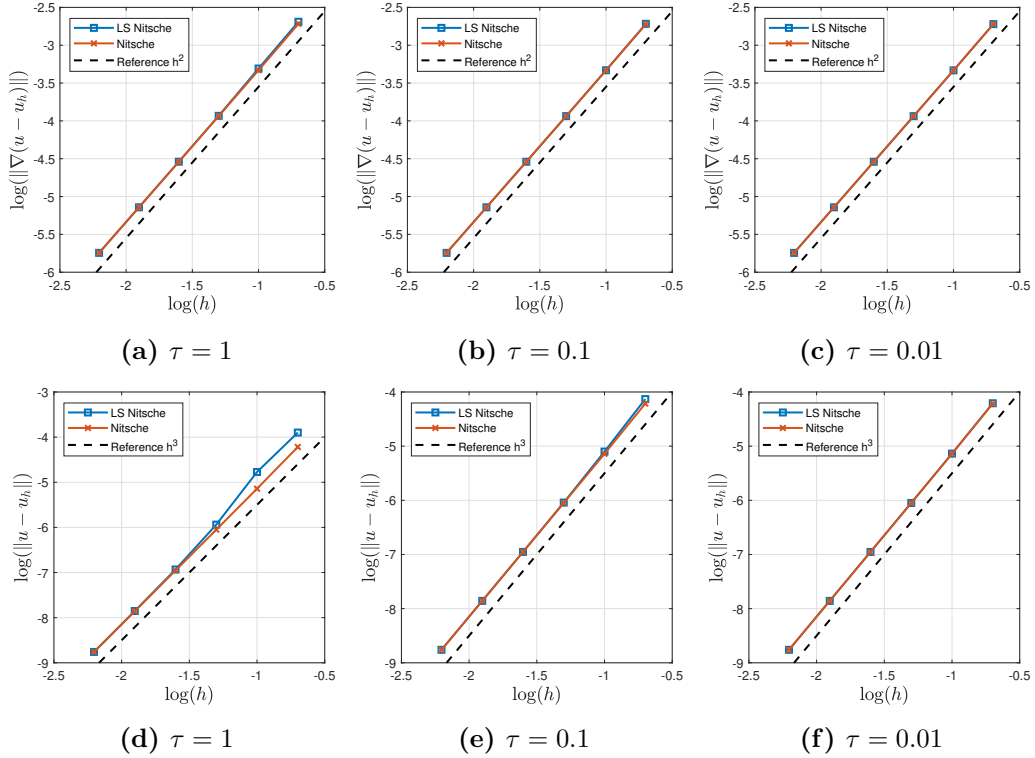


Figure 8: Convergence results for the square model problem with a perfectly fitted mesh.

Coercivity on $H^2(\Omega)$. The least squares stabilized Nitsche method is coercive on the full space $V = H^2(\Omega)$ rather than only on the finite element space V_h , which is conventionally the case for Nitsche methods. To illustrate this we keep the method fixed and study behavior of the smallest eigenvalues when refining the mesh. If the smallest eigenvalue is negative the method cannot be coercive. We fix the method based on a 10×10 mesh, meaning the parameter h and subdomain $\mathcal{T}_{h,\delta}$ are fixed in the method (2.7) and are thereby independent of the actual computational mesh, see Figure 12. As expected the results in Figure 13 show that the least squares stabilized Nitsche method maintains a positive smallest eigenvalue in every investigated case. The size of the smallest eigenvalue however approaches zero. The standard Nitsche method is only coercive on V_h and thus eventually attains negative smallest eigenvalues if the method is held fixed.

6 Conclusions

We have developed a new symmetric Nitsche formulation for cut C^1 elements that is coercive on $H^2(\Omega)$ and that does not rely on ghost penalties or choosing a very large penalty parameter in the Nitsche penalty term. Instead, the method is based on adding certain consistent least squares terms on, and in the vicinity of, the boundary. This new least square stabilized symmetric Nitsche method has the following notable features:

- The least squares stabilization terms are consistent and are only added elementwise.
- The method is coercive with respect to the energy norm on the full space $V = H^2(\Omega)$ rather than on the discrete space V_h as is the case in the analysis of the standard symmetric Nitsche method which rely on inverse inequalities on V_h .

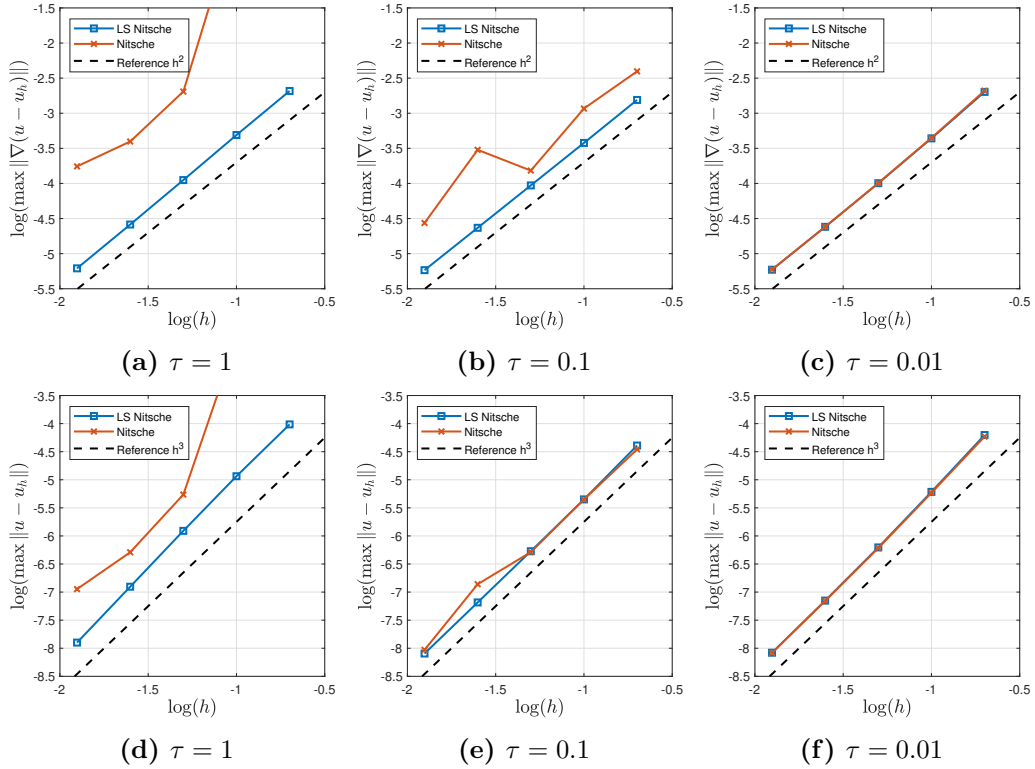


Figure 9: Worst case convergence for the circle model problem on cut meshes produced by shifting the background grid to 100 different positions for each mesh size. We use $\beta = 10$ and basis function removal is activated with $c = 0.01$. Note that we haven't ensured coercivity for the standard Nitsche method in the worst case cut scenarios. In typical cases lack of coercivity can be remedied by increasing the penalty parameter, for example by making τ smaller, and we indeed notice improved stability of the standard Nitsche method with smaller τ .

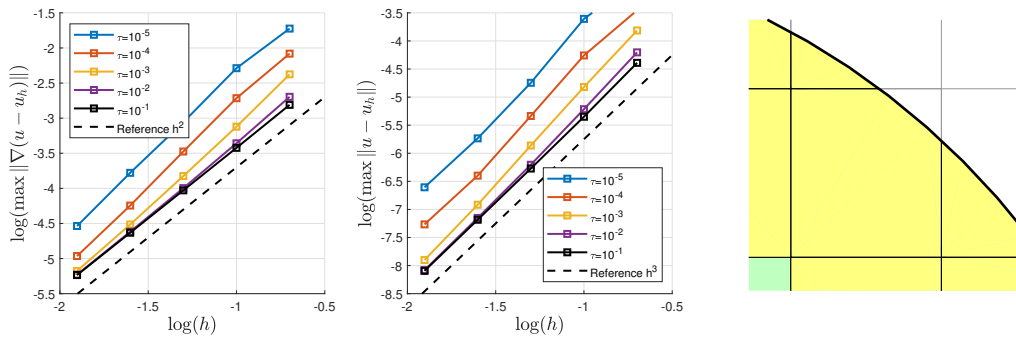


Figure 10: Worst case convergence using small values of τ in the least squares stabilized Nitsche method for the circle model problem. This corresponds to large values of the effective Nitsche parameter $\beta(1 + \tau^{-1})$. We use $\beta = 10$ and basis function removal is activated with $c = 0.01$. The standard Nitsche method yields close to identical results for these values of τ with the exception of $\tau = 0.1$ which is studied in Figure 9. We attribute the increasing errors when lowering τ to locking which is pronounced by the boundary being curved within cut elements as shown in the mesh detail on the right.

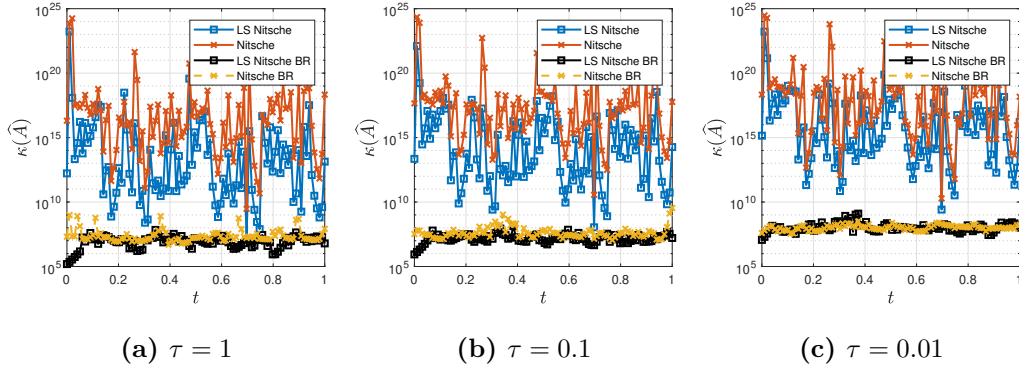


Figure 11: Stiffness matrix condition numbers in the unit circle model problem where the background grid is shifted based on the parameter t creating a variety of cut situations. Condition numbers after basis function removal with $c = 0.1$ are marked “BR”.

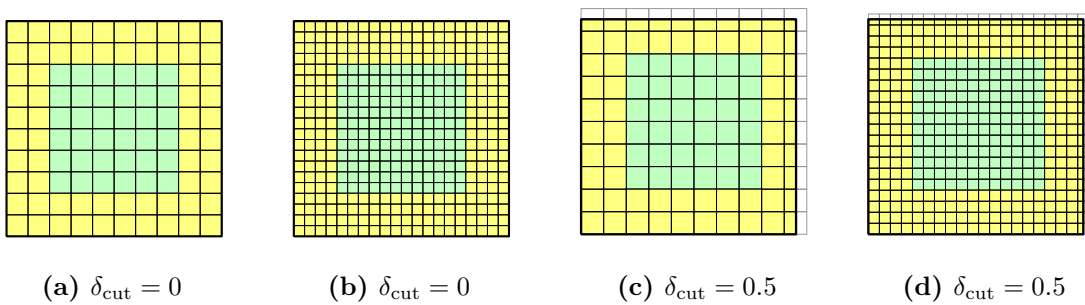


Figure 12: 10×10 and 20×20 meshes with the method fixed at 10×10 . Yellow indicates the fixed subdomain $\mathcal{T}_{h,\delta} \cap \Omega$ in the method. (a)–(b) One refinement of a fitted mesh. (c)–(d) One refinement of a cut mesh, preserving $\delta_{\text{cut}} = 0.5$. In this construction of cut meshes $\mathcal{T}_{h,\delta} \cap \Omega$ is not precisely fixed albeit converges to the corresponding domain in the fitted grid case.

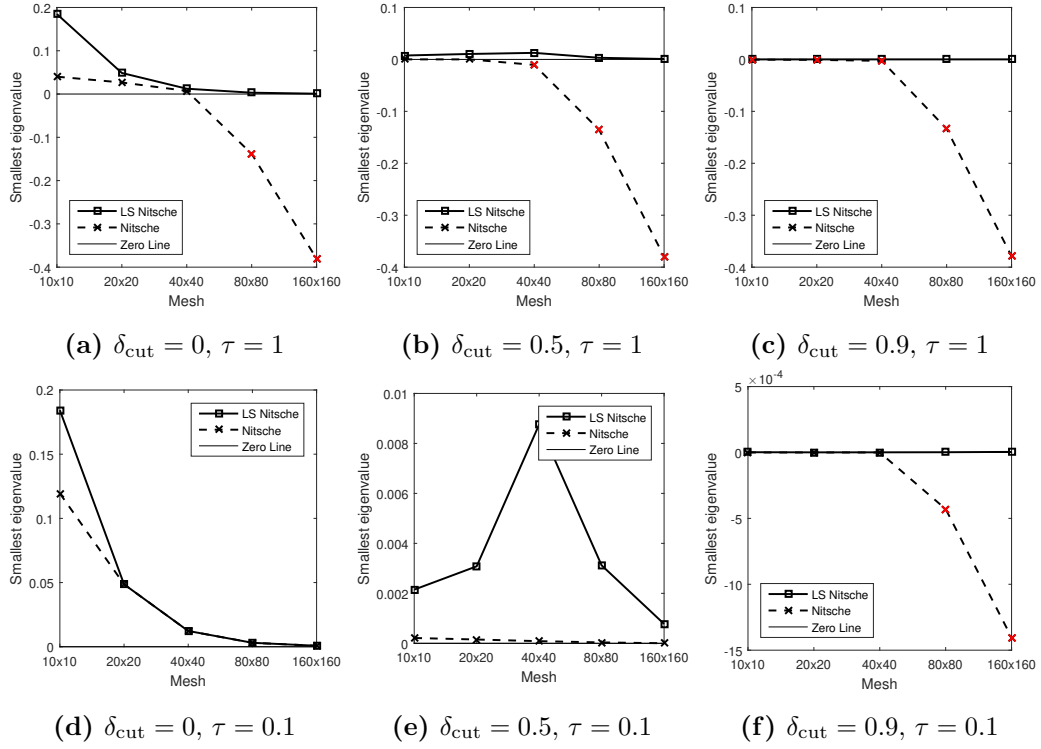


Figure 13: Smallest stiffness matrix eigenvalues versus mesh refinements when the method is fixed at 10×10 . That means that $\mathcal{T}_{h,\delta} \cap \Omega$ and h are fixed in the method and thus independent of the choice of mesh. Negative eigenvalues are displayed in red. The least squares stabilized Nitsche retains a positive smallest eigenvalue in all experiments.

- Since the intersection between elements and the domain Ω may be arbitrary small the $H^2(\Omega)$ coercivity only guarantee that the stiffness matrix is positive semidefinite. To ensure a positive definite stiffness matrix we employ the Basis Function Removal technique recently introduced in [10].
- In the numerical results we achieve very stable convergence results with respect to the cut situation even when using a penalty parameter which is only of moderate size. This is desirable in many cases where choosing a too large penalty parameter may introduce locking, for example when the boundary is non-trivial within cut elements, when using inhomogeneous boundary data, or in interface problems on non-matching grids. The τ parameter in the formulation allows for convenient adjustment of the penalty parameter size in the Nitsche penalty term while maintaining coercivity.

Acknowledgements. This research was supported in part by the Swedish Foundation for Strategic Research Grant No. AM13-0029, the Swedish Research Council Grants Nos. 2013-4708, 2017-03911 and the Swedish Research Programme Essence.

References

- [1] S. Badia, F. Verdugo, and A. F. Martín. The aggregated unfitted finite element method for elliptic problems. *ArXiv e-prints*, Sept. 2017.
- [2] Y. Bazilevs, L. Beirão da Veiga, J. A. Cottrell, T. J. R. Hughes, and G. Sangalli. Isogeometric analysis: approximation, stability and error estimates for h -refined meshes. *Math. Models Methods Appl. Sci.*, 16(7):1031–1090, 2006.
- [3] S. P. A. Bordas, E. Burman, M. G. Larson, and M. A. Olshanskii, editors. *Geometrically Unfitted Finite Element Methods and Applications*, volume 121 of *Lecture Notes in Computational Science and Engineering*. Springer Verlag, 2017.
- [4] E. Burman. Ghost penalty. *C. R. Math. Acad. Sci. Paris*, 348(21-22):1217–1220, 2010.
- [5] E. Burman, S. Claus, P. Hansbo, M. G. Larson, and A. Massing. CutFEM: discretizing geometry and partial differential equations. *Internat. J. Numer. Methods Engrg.*, 104(7):472–501, 2015.
- [6] J. A. Cottrell, T. J. R. Hughes, and Y. Bazilevs. *Isogeometric analysis*. John Wiley & Sons, Ltd., Chichester, 2009. Toward integration of CAD and FEA.
- [7] F. de Prenter, C. Lehrenfeld, and A. Massing. A note on the stability parameter in nitsches method for unfitted boundary value problems. *Comput. Math. Appl.*, 2018. Advance online publication.
- [8] F. de Prenter, C. Verhoosel, and H. van Brummelen. Preconditioning immersed isogeometric finite element methods with application to flow problems. *ArXiv e-prints*, Aug. 2017.
- [9] F. de Prenter, C. V. Verhoosel, G. J. van Zwieten, and E. H. van Brummelen. Condition number analysis and preconditioning of the finite cell method. *Comput. Methods Appl. Mech. Engrg.*, 316:297–327, 2017.
- [10] D. Elfverson, M. G. Larson, and K. Larsson. CutIGA with basis function removal. *Adv. Model. Simul. Eng. Sci.*, 5(6):1–19, 2018.
- [11] G. B. Folland. *Introduction to partial differential equations*. Princeton University Press, Princeton, NJ, second edition, 1995.
- [12] D. Gilbarg and N. S. Trudinger. *Elliptic partial differential equations of second order*. Classics in Mathematics. Springer-Verlag, Berlin, 2001. Reprint of the 1998 edition.
- [13] A. Hansbo, P. Hansbo, and M. G. Larson. A finite element method on composite grids based on Nitsche’s method. *M2AN Math. Model. Numer. Anal.*, 37(3):495–514, 2003.

- [14] A. Johansson and M. G. Larson. A high order discontinuous Galerkin Nitsche method for elliptic problems with fictitious boundary. *Numer. Math.*, 123(4):607–628, 2013.
- [15] T. Jonsson, M. G. Larson, and K. Larsson. Cut finite element methods for elliptic problems on multipatch parametric surfaces. *Comput. Methods Appl. Mech. Engrg.*, 324:366–394, 2017.
- [16] A. Massing, M. G. Larson, A. Logg, and M. E. Rognes. A stabilized Nitsche fictitious domain method for the Stokes problem. *J. Sci. Comput.*, 61(3):604–628, 2014.
- [17] J. T. Oden, I. Babūška, and C. E. Baumann. A discontinuous *hp* finite element method for diffusion problems. *J. Comput. Phys.*, 146(2):491–519, 1998.
- [18] J. Parvizian, A. Düster, and E. Rank. Finite cell method: *h*- and *p*-extension for embedded domain problems in solid mechanics. *Comput. Mech.*, 41(1):121–133, 2007.

Authors' addresses:

Daniel Elfverson, <code>daniel.elfverson@umu.se</code>	Mathematics and Mathematical Statistics, Umeå University, Sweden
Mats G. Larson, <code>mats.larson@umu.se</code>	Mathematics and Mathematical Statistics, Umeå University, Sweden
Karl Larsson, <code>karl.larsson@umu.se</code>	Mathematics and Mathematical Statistics, Umeå University, Sweden